Modeling Of Thermodynamic Properties Of H 2 And H 2 Mixtures Using A Three-Parameter Cubic Equation Of State

Clément Sevestre, Salaheddine Chabab, Julien Brocus, Christophe Coquelet

Modeling Of Thermodynamic Properties Of H_2 And H_2 Mixtures Using A Three-Parameter Cubic Equation Of State

Clément SEVESTRE[a], Salaheddine CHABAB[b,c], Julien BROCUS[a], Christophe COQUELET[a]

[a]*RAPSODEE, CNRS UMR 5203, Université de Toulouse, IMT Mines Albi, Campus Jarlard, Albi CT Cedex 09, 81013, France*
[b]*Universite de Pau et des Pays de l'Adour, E2S UPPA, LaTEP, Pau, 64000, France*
[c]*Universite de Pau et des Pays de l'Adour, E2S UPPA, CNRS, LFCR, UMR5150, Pau, 64000, France*

Abstract

Throughout the hydrogen value chain, industries increasingly rely on digital tools utilizing equations of state to develop safer, more efficient, and cost-effective processes. This paper compares the Peng-Robinson equation of state with volume translation (tc-PR EoS) and the Coquelet-El Abbadi-Houriez equation of state (CAH EoS), modified with the Feymann Hibbs correction to the covolume, to account for the quantum swelling phenomenon. The models were used to predict density, residual enthalpy, and Joule-Thomson coefficients over a temperature range of 20 to 353 K. It has been applied to binary mixtures relevant to the hydrogen industry, including H_2/CO_2, H_2/CO, H_2/CH_4, and H_2/N_2. Model parameters were fitted to liquid-vapor equilibrium (VLE) data using the generalized Wong-Sandler (gWS) and van der Waals (vdW) classical mixing rules. The performance of the models in representing VLE data and densities over a wide range of thermodynamic conditions was assessed. These models can help design processes for hydrogen production, transport and use.

Keywords: Cubic three-parameter equation of state, normal Hydrogen, Thermodynamic properties, Vapor-liquid equilibrium

---

1. Introduction

Hydrogen is a molecule that could serve as an energy vector in the coming decades, potentially replacing fossil fuels. By 2050, Europe is projected to consume approximately $2760\ \mathrm{TW{\cdot}h}$ of hydrogen, primarily for industrial, transportation, and heat production sectors [1]. Currently, hydrogen production is predominantly achieved through coal or lignite gasification (black hydrogen),

processes that offer efficiencies ranging from 60 to 75% [2]. To reduce carbon dioxide emissions, alternative methods such as electrolysis and methane cracking are being developed. Electrolysis is gaining support in countries with substantial solar or nuclear energy resources, achieving efficiencies of up to 90% [3]. In addition, the production of hydrogen from biomass (green hydrogen) is an emerging technology, producing a gas that forms syngas (H_2+CO) after purification [4]. Another approach involves pyrolyzing methane (turquoise hydrogen) at high temperatures to produce solid carbon and hydrogen [5][6]. Despite these advancements, hydrogen transport and storage remain major challenges, as the development is hampered by hydrogen's instability [7]. Liquefaction, while facilitating easier transport, consumes more than 30% of the hydrogen's energy content and incurs additional losses from evaporation (boil-off effect) [8]. To address these issues, projects focused on converting hydrogen into ammonia or methanol are underway, as these substances are easier to transport and store in liquid form [9]. These compounds also mitigate risks associated with pressure and evaporation and are compatible with current technologies [10]. Pure hydrogen is mainly used in the transportation sector as a substitute for hydrocarbon fuels. It also finds applications in the aerospace industry as a fuel coupled with helium for cooling, and in steelmaking for welding operations, owing to its properties in generating hot arcs and industrial plasmas [11][12]. The growing demand for industrial applications using hydrogen underscores the importance of developing simple and efficient thermodynamic models [13][14][15]. The production, transport, and use of hydrogen require a deep understanding of the associated physical and quantum phenomena. Although industrial-scale hydrogen production is advancing, current knowledge about its behavior remains limited due to its physical complexity. Studies on interaction potentials have highlighted the necessity of considering "quantum swelling", where the effective size of particles increases at low temperatures due to the wave-like nature of particles becoming more pronounced as the de Broglie thermal wavelength increases [16]. Currently, the focus in hydrogen modelling is on its application in the cryogenic range (from 0 to 150 K), aiming to develop simple cryogenic models adaptable to various industrial applications. The most precise equations of state available today are often too complex for direct industrial use, relegating them mainly to foundational roles in unit operation design. Therefore, cubic equations of state are favored for their simplicity and effectiveness, with the Peng-Robinson equation being the most widely used [17]. These cubic equations are also useful

in computational fluid dynamics (CFD) simulations [18][19], where equation simplicity is crucial for maintaining the stability and speed of system resolution. However, the two parameter equations of state are limited in their representation of the density of the liquid, which is why Peneloux volume translation is commonly applied to the liquid phase. [20]. In their recent work, Quinzio et al. [21] investigated the benefits of adding a third parameter to a cubic EoS. Interestingly, they showed that a third parameter not only improves the predictions of equilibrium properties of pure compounds, but also considerably improves those of mixtures, especially asymmetric ones, where 2-parameter EoSs often fall short, even with an adjusted binary interaction parameter.

This paper aims to demonstrate the predictive performance of normal hydrogen thermodynamic properties using a cubic equation of state (EoS) through two approaches: quantum corrected translated-consistent Peng-Robinson (tc-PR) with volume translation and Coquelet-El Abbadi-Houriez (CAH). This comparison allows for an in-depth evaluation of the advantages of two- and three-parameter cubic equations of state. Initially, the model will be presented, along with adjustments made to account for the "quantum swelling" phenomenon of normal hydrogen. Subsequently, the performance of the model will be assessed by comparing the prediction of key thermodynamic properties of pure normal hydrogen with those obtained using the quantum corrected tc-PR EoS. Finally, to evaluate the model's performance in modeling mixtures properties, the van der Waals mixing rule (vdW-MR) and the generalized Wong-Sandler mixing rule (g-WS MR) will be employed. These mixing rules will be used to predict the liquid-vapor equilibrium of binary mixtures containing hydrogen, as well as the density for a given hydrogen composition.

Nomenclature

Acronym

ARD Average Relative Deviation

BIAS Relative deviation

BIP Binary Interaction Parameter

BRP Binary Repulsion Parameter

CAH Coquelet-El Abbadi-Houriez

CFD Computational Fluid Dynamics

EoS Equation of state

g-WS MR generalized Wong-Sandler Mixing rule

GWP Global Warming Potential

NRTL No Random Two Liquids

SRK Soave-Redlich-Kwong

tc-PR translated-consistent Peng-Robinson

vdW MR van der Waals Mixing rule

VLE Vapor Liquid Equilibrium

Chemistry compound

CH_4	Methane
CO	Carbon monoxide
CO_2	Carbon dioxide
He	Helium
H_2	Normal Hydrogen
H_2O	Water
N_2	Nitrogen

Greek letter

α_{ij}	NRTL alpha parameter α_{TWU} Alpha function
β	Beta function
Λ	Wong-Sandler mixing rule parameter
Λ_i	Wong-Sandler mixing rule parameter
μ	Joule-Thomson coefficient ($\mathrm{MPa \cdot K^{-1}}$)
Ω	Acentric factor
Ω_a	Substance depending factor
Ω_b	Substance depending factor
Ω_c	Substance depending factor
ρ	Density ($\mathrm{kg \cdot m^{-3}}$)
ρ_{satl}	Saturation liquid density ($\mathrm{m^3 \cdot mol^{-1}}$)
ρ_v^{sat}	Saturation vapor density ($\mathrm{m^3 \cdot mol^{-1}}$)
ρ_c	Critical density ($\mathrm{kg \cdot m^{-3}}$)
τij	NRTL binary interaction parameter
ξ	Numerical weight

Symbol

A	Feynman-Hibbs parameter (K)
a	Cohesive energy parameter ($\mathrm{J \cdot mol^{-1}}$)
A_∞^{ex}	Excess Helmholtz free energy ($\mathrm{Pa \cdot m^3 \cdot mol^{-1}}$)
A_{ij}	Wong-Sandler mixing rule numerical parameter ($\mathrm{K^2}$)
$A_{k,ij}$	BIP numerical parameter ($\mathrm{K^{-1}}$)
B	Feynman-Hibbs parameter (K)
b	Covolume parameter ($\mathrm{m^3 \cdot mol^{-1}}$)
B_{ij}	Wong-Sandler mixing rule numerical parameter (K)
$B_{k,ij}$	BIP numerical parameter
c	CAH parameter ($\mathrm{m^3 \cdot mol^{-1}}$)
C_{ij}	Wong-Sandler mixing rule numerical parameter
cp_{res}	Residual isobaric heat capacity ($\mathrm{kJ \cdot kg^{-1} \cdot K^{-1}}$)
D	Wong-Sandler mixing rule parameter

D_{ij}	Wong-Sandler mixing rule numerical parameter
E_{ij}	Wong-Sandler mixing rule numerical parameter (K^{-1})
F_{ij}	Wong-Sandler mixing rule numerical parameter (K^{-2})
G_{ex}	Gibbs free energy ($Pa \cdot m^3 \cdot mol^{-1}$)
h_{res}	Residual enthalpy ($kJ \cdot kg^{-1}$)
k_{ij}	BIP parameter
L	Twu parameter
l_{ij}	BRP parameter
M	Twu parameter
N	Twu parameter
N_c	Number of compounds
N_{exp}	Number of experimental data points
N_{ref}	Number of data points
P	Pressure (MPa)
P_{sat}	Saturation pressure (MPa)
P_c	Critical pressure (MPa)
P_r	Reduced pressure
P_{exp}	Experimental pressure
Q	Wong-Sandler mixing rule parameter
R	Universal gas constant ($J \cdot K^{-1} \cdot mol^{-1}$)
s_{res}	Residual entropy ($kJ \cdot kg^{-1} \cdot K^{-1}$)
T	Temperature (K)
T_c	Critical temperature (K)
T_r	Reduced temperature (K)
T_t	Triple point temperature (K)
u_1	EoS parameter ($m^3 \cdot mol^{-1}$)
u_2	EoS parameter ($m^3 \cdot mol^{-1}$)
$u_{1,opt}$	EoS optimal parameter ($m^3 \cdot mol^{-1}$)
$u_{2,opt}$	EoS optimal parameter ($m^3 \cdot mol^{-1}$)
v	Molar volume ($m^3 \cdot mol^{-1}$)
v_t	Volume translation ($m^3 \cdot mol^{-1}$)
w	Speed of sound ($m \cdot s^{-1}$)
x	Liquid molar fraction
X_{cal}	Calculated thermodynamic property
X_{exp}	Experimental thermodynamic property
x_{exp}	Experimental liquid molar fraction
y	Vapor molar fraction
y_{exp}	Experimental vapor molar fraction
Z	Compressibility factor
Z_c	Critical compressibility factor
$Z_{c,opt}$	Adjusted critical compressibility factor

2. Model presentation

The general form of the cubic equations of state is defined within the Eq (1) where (P) is the pressure, (R) is the gas constant, (T) is the temperature and (v) is the molar volume, (Ω_a), (Ω_b), (u_1) and (u_2) are numerical constants that depend on the EoS used. The cohesive energy parameter (a) and the covolume (b) are defined by Eqs (2), (3) where (T_c) is the critical temperature, (P_c) is the critical pressure, (α_{TWU}) is the α-function and (β) is the Feynman-Hibbs function.

$$P = \frac{RT}{v-b} - \frac{a}{v^2 + u_1 bv + u_2 b^2} \tag{1}$$

$$a = \Omega_a \frac{R^2 T_c^2}{P_c} \alpha(T_r) \tag{2}$$

$$b = \Omega_b \frac{RT_c}{P_c} \beta(T_r) \tag{3}$$

A paper has demonstrated that the constants u_1 and u_2, defined, yield optimal vapor liquid equilibrium and density modeling results when $u_{1,opt} = 2.10$ and $u_{2,opt} = -0.75$ [22]. In the case of the tc-PR EoS, the values are very close ($u_1 = 2$ and $u_2 = -1$).

To get as close as possible to the optimum values, the model presented stems from the fusion of a three-parameter cubic equation designed for refrigerant modeling and work on modeling the quantum effects of normal hydrogen. The CAH EoS is a modified three-parameter Patel-Teja EoS [23]. To achieve better results on thermodynamic properties than the tc-PR EoS, the constants (u_1) and (u_2) are calculated using Eqs (4) to (9) based on the corrected critical compressibility factor for each pure substance. Parameters (u_1) and (u_2) are defined by the relation (4):

$$u_1 + u_2 = 0 \tag{4}$$

Where (u_1) is defined by the expression (5):

$$u_1 = 1 + \frac{c}{b} \tag{5}$$

The parameters (c) is defined by the Eq (6).

$$c = \Omega_c \frac{RT_c}{P_c} \tag{6}$$

The parameters (Ω_a), (Ω_b), and (Ω_c) are defined by equations (7) to (9) where the critical compressibility factor ($Z_{c,opt}$) becomes a component-specific parameter.

$$\Omega_{\mathrm{a}} = 1 - 3Z_{c,opt}(1 - Z_{c,opt}) + 3\big(1 - 2Z_{c,opt}\big)\Omega_b + 2\Omega_b^2 \tag{7}$$

$$\Omega_b^3 + \big(1 - 3Z_{c,opt}\big)\Omega_b^2 + 3Z_{c,opt}^2 - Z_{c,opt}^3 = 0 \tag{8}$$

$$\Omega_c = 1 - 3Z_{c,opt} \tag{9}$$

The performance of CAH EoS will be compared with the tc-PR EoS defined by Eq (S1) in supplementary materials section [17]. In the subsequent parts of this paper, the Peneloux volume translation (v_t) is incorporated into the tc-PR EoS in all modeling and defined by Eq (10) [20]. However, this volume translation (v_t) increases density and residual enthalpy modelling.

$$P = \frac{RT}{v - b} - \frac{a}{(v + v_t)(v + v_t + b) - b(v + v_t - b)} \tag{10}$$

3. Pure compounds modeling

3.1. The α and β function selected

The generalized Twu et al. α-function (α_{TWU}), defined by Eq.(11), is selected, where (L), (M) and (N) are component-specific parameters and (T_r) is the reduced temperature [24].

$$\alpha_{TWU}(T_r) = T_r^{N(M-1)} \exp\left(L(1 - T_r^{MN})\right) \tag{11}$$

The model must take into account the "quantum swelling phenomenon" of quantum molecules. To address these phenomena, Aasen et al. proposed an improvement based on Feynman-Hibbs quantum-correction [16] [25]. For this paper, the Feynman–Hibbs correction is applied to the covolume in the case of normal hydrogen and helium, defined by Eq (12), where (A) and (B) are component-specific parameters. This β-function should be a decreasing function and is intuitively expected to tend towards 1 for $T > T_r$.

$$\beta = \frac{\left(1 + \frac{A}{B+T}\right)^3}{\left(1 + \frac{A}{B+T_c}\right)^3} \quad (12)$$

3.2. Numerical parameter adjustment methodology

For each component studied, the properties used for each component are described in Table 1 where (ρ_c) is the critical density, (ω) is the acentric factor and (T_t) is the triple point temperature. The nonlinear optimization method "Fmincon" available in Matlab version 2023b software [26][27][28][29] was selected to adjust each numerical coefficient, including (L), (M), (N), ($Z_{c,opt}$), as well as (A) and (B) for the quantum components for each compound listed in Table 1. These parameters are adjusted by minimizing the difference between the value provided by CAH EoS and the value of the reference equation, the objective function is defined by the Eq (13). The chosen thermodynamic properties are the saturated vapor pressures and the saturation liquid densities given by the reference equation of each component.

$$F_{obj} = \sum_{i=1}^{N_{ref}} \zeta \left(\frac{X_{ref,i} - X_{cal,i}}{X_{ref,i}} \right)^2 \quad (13)$$

Where (ξ) is the weight that is adjusted to prioritize the accurate representation of certain thermodynamic properties over others, (N_{ref}) is the number of data points and (X) is ($P^{sat}(T)$) (with $\xi = 0.8$) and ($\rho_l^{sat}(T)$) (with $\xi = 0.2$). The numerical parameters are adjusted by minimising the objective function considering each component "reference" EoS [30][31][32][33][34][35][36][37]. The accuracy of each thermodynamic properties predicted by the reference EoS for each component are mentioned in Table 2. More details on uncertainty values can be found in the corresponding reference paper. The optimized values used for each component are gathered in Table 2. For the non-quantum components, the variables (A) and (B) are set to zero.

Table 1: Critical data for each component.

Name	T_c (K)	P_c (MPa)	ρ_c (kg·m^{-3})	ω	T_t (K)	Reference
H_2	33.145	1.2964	31.262	-0.219	13.957	[30]
He	5.1953	0.22832	69.58	-0.3836	2.1768	[31]
CO_2	304.13	7.773	467.6	0.22394	216.59	[32]
CO	132.86	3.494	303.91	0.0497	68.16	[33]
Ar	150.69	4.863	535.6	-0.00219	83.806	[34]
N_2	126.19	3.3958	313.3	0.0372	63.151	[35]
H_2O	647.1	22.064	322.0	0.3443	273.16	[36]
CH_4	190.56	4.5992	162.66	0.01142	90.964	[37]

Table 2: Numerical settings used for Eqs. (11) and (12) for each component are applied to CAH EoS.

	Numerical parameter						Reference EoS accuracy						
Component	**L**	**M**	**N**	**Zc,opt**	**A(K)**	**B(K)**	**Δρ(%)**	**Δw(%)**	**Δcp(%)**	**ΔPsat(%)**	**P-range (MPa)**	**T-range (K)**	**ref**
H_2	-0.0108	-0.039	0.0352	0.3133	0.8277	0.2147	0.04	0.5	1.0	0.2	0-100	250-450	[30]
He	0.3711	2.174	0.2668	0.3202	1.1518	4.3821	0.2	0.2	2.0	0.02	0-50	50-200	[31]
CO2	0.286	0.8928	1.3935	0.2911			0.05	1.0	1.5	0.012	0-30	0-523	[32]
CO	4.4434	0.0945	0.2129	0.3			1.0	-	2.0	0.2	0-100	0-500	[33]
Ar	0.4434	0.7897	0.4312	0.3042			0.03	1.0	2.0	0.04	0-30	90-450	[34]
N_2	2.6974	1.337	0.085	0.3013			0.02	1.5	2.0	0.02	0-30	240-523	[35]
H_2O	0.2051	0.6371	0.8639	0.2459			0.1	0.15	0.2	0.025	273-423	0-10	[36]
CH_4	2.2932	3.6516	0.0438	0.3009			0.07	0.3	1.0	0.07	0-50	91-350	[37]

The values used for quantum corrected tc-PR EoS are drawn from various articles:

- Aasen et al. [16] for quantum compounds.
- The general formula of Twu et al. parameters dependent on the acentric factor of Privat and al. [24] for water.
- Le Guennec et al. [38] for other.

These values are available in Table S1 in supplementary material section. For quantum corrected tc-PR EoS, the optimization of the volume translation of water was carried out by fixing the parameters of the Twu et al. function and minimizing the gap between the liquid density curve of water at saturation calculated by the reference equation and the one from quantum corrected tc-PR EoS over the temperature range from the triple to the critical point. The volume translation value for water obtained is $v_{t,\mathrm{H^2O}} = 2.44 \times 10^{-3}\ \mathrm{m^3{\cdot}kg^{-1}}$.

3.3. Results and discussion

The optimized values for normal hydrogen closely align with the reference equation of state, as illustrated in Figures 1a and 1b.

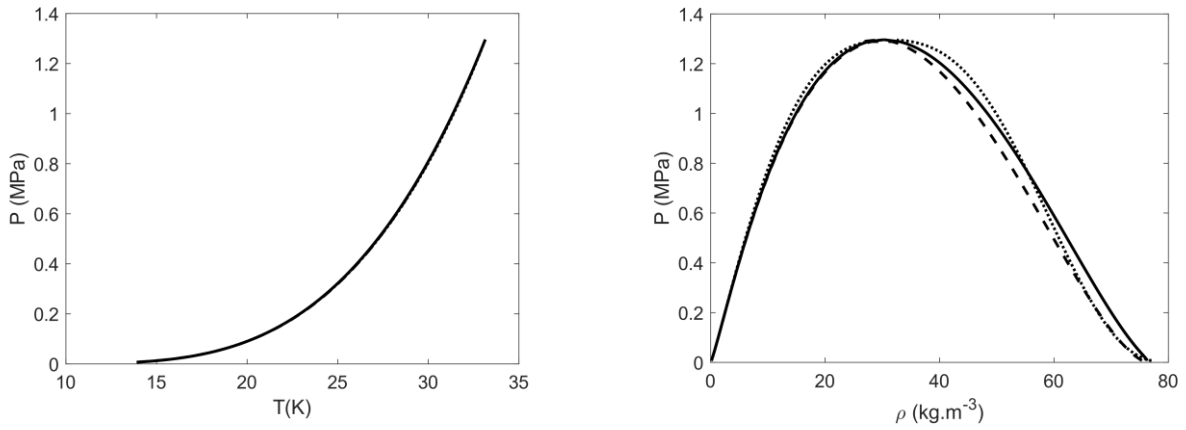

(a) Pressure (b) Density

Figure 1: Saturation line for pure normal hydrogen. Solid line: CAH EoS modeling, Dashed line: Quantum corrected tc-PR EoS, Dotted line: fundamental normal hydrogen EoS modeling [30].

A strong agreement is observed between the calculated values from the reference EoS and those predicted by our model, spanning from the triple point to the critical point.

The model's performance is quantified using the relative deviation (BIAS) and the average relative deviation (ARD), as defined in Eqs. (14) and (15) respectively where (X) is a thermodynamic property.

$$BIAS(X)\% = \frac{100}{N_{ref}} \sum_{i=1}^{N_{ref}} \frac{X_{ref,i} - X_{cal,i}}{X_{ref,i}} \tag{14}$$

$$ARD(X)\% = \frac{100}{N_{ref}} \sum_{i=1}^{N_{ref}} \left| \frac{X_{ref,i} - X_{cal,i}}{X_{ref,i}} \right| \tag{15}$$

The calculated BIAS and ARD values for each component studied are summarized in Table S2 in supplementary material section. The CAH EoS provides superior predictions for the saturation pressure and liquid density of pure normal hydrogen compared to those from the quantum corrected tc-PR EoS. However, the dispersion in liquid density remains comparable between the two models.

The behavior of the α-function for CAH EoS, depicted in Figure 2a, shows a gradual decline towards zero, adhering to the monotonic decrease condition for alpha functions as outlined by Le Guennec et al [38]. In contrast, the α-function for the quantum corrected tc-PR EoS exhibits a bell-shaped form below $50\ \mathrm{K}$, transitioning to a decreasing trend at higher temperatures. While this does not strictly comply with the alpha function requirements, it is acceptable for quantum pure substances [24].

In this paper, the validation of the numerical parameters for each component is based on two elements, the prediction of the pressure and density at saturation. These predictions are comparable to the quantum corrected tc-PR EoS and the behaviour of the alpha function respects the conditions given by Le Guennec et al. for helium and normal hydrogen.

The Beta function behavior for CAH EoS, shown in Figure 2b, indicates that beyond $150\ \mathrm{K}$, the Feynman-Hibbs correction remains nearly constant at $\beta = 0.985$, rendering the correction negligible outside the cryogenic range. The critical compressibility factor optimization in the CAH model mitigates the correction impact, which is significant only at temperatures below $150\ \mathrm{K}$.

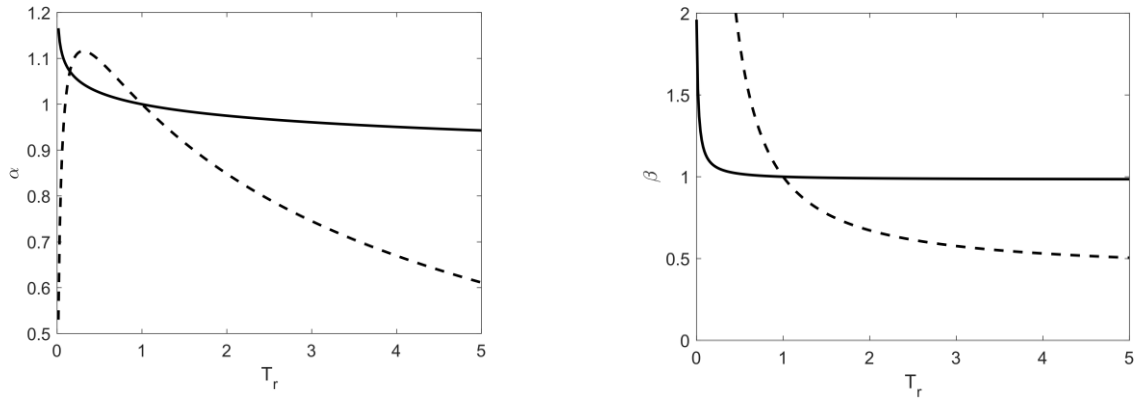

(a) α function (b) β function

Figure 2: Numerical function lines depend on temperature for pure normal hydrogen. Solid line: CAH EoS modeling, Dashed line: Quantum corrected tc-PR EoS modeling (using parameters from Table S1).

The main thermodynamic properties predicted by the models are described in Figure 3 and the details are referenced in Table 3. The quantum corrected tc-PR EoS more accurately predicts density at high pressures and low temperatures, whereas CAH EoS maintains an error margin below 4.1% across the entire range. Near the critical point, CAH EoS predictions are comparable to those of quantum corrected tc-PR EoS, as demonstrated in Figure S4 and Table S4 in supplementary material section. Residual enthalpy predictions are superior with CAH EoS at low temperatures, but this accuracy diminishes above $20\ \mathrm{K}$. Residual entropy modeling yields better results with a maximum deviation of 11% for CAH EoS, compared to 32% for quantum corrected tc-PR EoS. At high temperatures, CAH EoS provides a better model for the residual molar heat capacity at constant pressure, albeit with lower overall precision. Speed of sound modeling accuracy is improved, with deviations under 4% above $105\ \mathrm{K}$ using CAH EoS. The Joule-Thomson coefficient is also better represented with CAH EoS, although both models exhibit limitations in this regard. Overall, while the CAH EoS has limitations, it offers improvements in the modelling of various thermodynamic properties over a wide pressure and temperature range.

The inclusion of volume translation in the quantum corrected tc-PR EoS significantly enhances the accuracy of density and residual enthalpy predictions. However, it negatively affects the modeling of other thermodynamic properties. Without volume translation, the quantum corrected tc-PR EoS provides better predictions for residual entropy, constant pressure heat capacity, speed of sound, and the Joule-Thomson coefficient, as detailed in supplementary material section.

Conversely, the CAH EoS, while slightly degrading the accuracy of density and residual enthalpy predictions, allows for reasonably accurate modeling of all thermodynamic properties. Pure component vapor pressure and liquid densities at saturation calculated by the CAH EoS are compared to available experimental data of pure normal hydrogen and helium in supplementary material section.

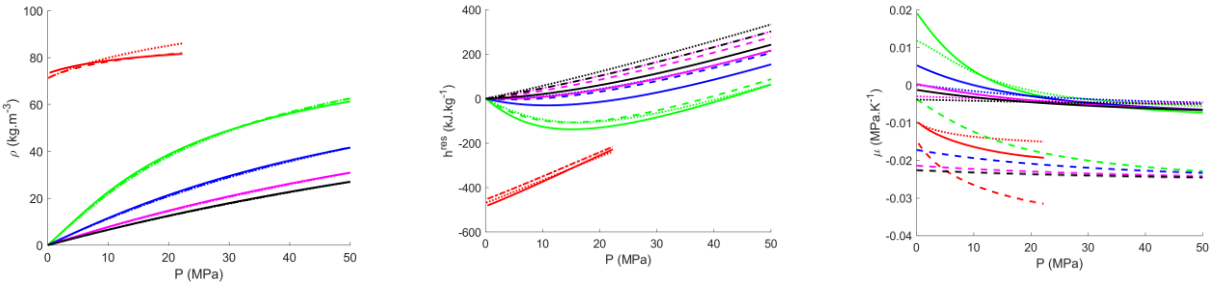

(a) *Density* (a) *Residual enthalpy* (c) *Joule-Thomson coefficient*

Figure 3: Thermodynamic properties of pure normal hydrogen as a function of pressure at 20 (red), 105 (green), 200 (blue), 298, (purple) and 353 (black) K. Solid line: CAH EoS modeling, Dashed line: Quantum corrected tc-PR EoS modeling, Dotted line: fundamental normal hydrogen EoS modelling [30].

Table 3: Comparison of quantum corrected tc-PR EoS and CAH EoS performance for pure normal hydrogen based on fundamental normal hydrogen EoS modeling [30]. Symbol ∅ stands for a percentage greater than 100 %.

EoS	Quantum corrected tc-PR						CAH					
T (K)	20	105	200	298	353	Avg	20	105	200	298	353	Avg
BIAS ρ	4.0	-0.56	-0.75	-0.52	-0.39	0.36	3.4	-1.3	-1.8	-1.2	-0.93	-0.37
ARD ρ	4.0	0.60	0.75	0.52	0.39	1.3	4.1	2.0	1.8	1.2	0.93	2.0
BIAS h^{res}	6.8	-1.1	22	17	15	12	0.8	-27	54	54	48	26
ARD $hres$	6.8	21	22	17	15	16	3.7	34	54	54	48	39
BIAS s^{res}	32	24	23	21	20	24	9.0	11	3.6	-3.0	-6.3	2.9
ARD $sres$	32	24	23	21	20	24	9	11	3.6	3.4	6.6	6.7
BIAS cp^{res}	90	24	29	30	31	41	-21	31	17	4.1	-3.3	5.6
ARD $cpres$	90	24	29	30	31	41	21	31	20	13	12	19
BIAS w	77	36	22	16	14	33	-10	1.9	0.46	-0.13	-0.15	-1.6
ARD w	77	36	22	16	14	33	13	4.0	2.2	1.2	1.0	4.3
BIAS μ	-83	∅	∅	∅	∅	-83	-19	-30	-13	1.2	-1.7	-13
ARD μ	83	∅	∅	∅	∅	83	19	34	30	28	22	27

4. Mixtures modeling

4.1. van der Waals mixing rule

To model hydrogen with other components while avoiding complicating the calculations, the optimized critical compressibility factors are kept constant for each pure component in mixtures. The parameters (a) and (b) of the equation of state are recalculated according to the classic van der Waals Mixing Rules (vdW MR). These parameters are computed using Eqs. (16) to (19) where (x_i) is the molar fraction of the compound i, (N_c) is the number of compounds, (k_{ij}) is the binary interaction parameters (BIP) and (l_{ij}) is binary repulsion parameters (BRP) between the compound i and the compound j [39].

$$a = \sum_{i=1}^{N_c} \sum_{j=1}^{N_c} x_i x_j a_{ij} \tag{16}$$

$$a = \sqrt{a_i a_j}(1 - k_{ij}) \tag{17}$$

$$b = \sum_{i=1}^{N_c} \sum_{j=1}^{N_c} x_i x_j b_{ij} \tag{18}$$

$$b = \frac{b_i + b_j}{2}(1 - l_{ij}) \tag{19}$$

The parameter (c) is calculated using the classical linear combination rule defined by equation (20).

$$c = \sum_{i=1}^{N_c} x_i c_i \tag{20}$$

For tc-PR EoS, the volume translation is defined by Eq (21) [40].

$$v_t = \sum_{i=1}^{N_c} x_i v_{t,i} \tag{21}$$

For each mixture, the binary interaction parameters (BIP) and binary repulsion parameters (BRP) were regressed for each isotherm using an optimization program in Matlab version 2023b software. The program minimizes the objective function defined by Eq (13), where (N_{ref}) is the number of data points, $\xi = 1$, (X) denotes the experimental vapor fraction (y_{exp}) and the experimental pressure (P_{exp}), respectively, for each isotherm. Each BIP was optimized for each isotherm, with the BRP considered constant for each compound. For helium, the values reported by Aasen et al. [16] for modeling with the quantum corrected tc-PR EoS were utilized.

A linear variation of the BIP as a function of temperature is considered, as described by Eq. (22) and illustrated in Figure S6 in supplementary material section. For other compounds, the BIP remains nearly constant with temperature, and the values of these coefficients are presented in Table 4.

$$k_{ij} = A_{k,ij} T + B_{k,ij} \tag{22}$$

Table 4: Value for Eq (22) and BRP (l_{ij}) for each compound.

	Quantum corrected tc-PR			CAH		
	$A_{k,ij}$	$B_{k,ij}$	l_{ij}	$A_{k,ij}$	$B_{k,ij}$	l_{ij}
H_2/He	0	0.17	-0.16	-0.01	0.495	-0.08
H_2/H_2O	6.91×10^{-3}	2.61	0.11	2.87×10^{-3}	-0.828	0.25
H_2/CO_2	0	0.14	0	0	0.13	0
H_2/CO	0	0.03	0	0	0.03	0
H_2/N_2	0	0.04	0	0	0.052	0
H_2/CH_4	0	0.01	0	0	0.032	0
H_2/Ar	0	-0.04	0	0	-0.037	0

4.2. Wong-Sandler mixing rule

To improve the calculation of phase equilibrium, particularly in mixtures, the Wong-Sandler mixing rules are considered [41]. The advantage of this type of mixing rule is that it retains the symmetrical ($\varphi - \varphi$) approach, which is suitable for high-pressure conditions, while also incorporating the flexibility offered by activity coefficient models. This coupling defined by the Eq (23) is achieved by equating the excess Helmholtz free energy at the infinite pressure state (A_{∞}^{ex}) with the excess Gibbs free energy (G^{ex}) derived from an activity model.

$$A_{\infty}^{ex} = G^{ex} \tag{23}$$

The generalized form of the Wong-Sandler mixing rules (g-WS MR), recently developed by Chabab et al. [42], was employed in this work. This generalized formulation is applicable to all types of two- and three-parameter cubic EoS. The g-WS MR are defined by the Eqs (24) and (25) where the parameters (Λ) and (Λ_i) depend on EoS used.

$$a = \frac{QDRT}{1 - D} \tag{24}$$

$$b = \frac{Q}{1 - D} \tag{25}$$

Where (D) and (Q) are defined by the Eqs (26) and (27)

$$D = \frac{\frac{A_{\infty}^{ex}}{RT} + \sum_{i=1}^{N_c} x_i \frac{a_i}{RTb_i} \Lambda_i}{\Lambda} \tag{26}$$

$$Q = \sum_{i=1}^{N_c} \sum_{j=1}^{N_c} x_i x_j \left(b_i - \frac{a_i}{RT} \right)_{ij} \tag{27}$$

For two-parameter cubic equations of state (EoS), such as van der Waals (vdW), Soave Redlich-Kwong (SRK), and Peng-Robinson (PR), the parameters (Λ) and (Λ_i) are equal and constant. However, for cubic equations of state with more than two parameters, (Λ) and (Λ_i) are not necessarily equal or constant and are dependent on the critical compressibility factor (Z_c). The procedure for calculating the various parameters and their corresponding derivatives, which are required to compute the fugacity coefficients, is detailed by Chabab et al. . In this work, the excess energy is obtained using the well-known activity model NRTL, developed by Renon and Prausnitz [43], defined by the Eq (28) where (τ_{ij}) is the NRTL binary interaction parameters and (α_{ij}) is the NRTL alpha parameter, fixed at 0.3.

$$\frac{A_\infty^{ex}}{RT} = \sum_{i=1}^{N_c} x_i \left[\frac{\sum_j x_j \tau_{ij} \exp\left(-\alpha_{ij}\tau_{ij}\right)}{\sum_j x_j \exp\left(-\alpha_{ij}\tau_{ij}\right)} \right] \tag{28}$$

Given the multiplicity of possible solutions, each set of optimized parameters was used to model densities, with the sets yielding consistent density modelling data being selected. In the optimization study of the H_2/CO_2 binary mixture, the parameters adjusted using the Fandino parameters [44], rather than those from Street [45], resulted in a consistent set of BIP while maintaining accuracy in density calculations. It was also observed that the parameter values obtained were lower when using the CAH EoS compared to the quantum corrected tc-PR EoS, suggesting that the CAH EoS more accurately accounts for molecular interactions. Consequently, the quality of the experimental data is crucial for accurately calibrating the models. For other mixtures, classical vapor-liquid equilibrium (VLE) data were employed. However, due to the instability of the parameter sets, a temperature dependency, as defined by Eqs (29) and (30), was necessary where (A_{ij}), (B_{ij}), (C_{ij}), (D_{ij}), (E_{ij}) and (F_{ij}) are adjusted numerical parameters. The parameters were optimized using literature data and are listed in Tables 5 and 6.

$$k_{ij} = \frac{A_{ij}}{T^2} + \frac{B_{ij}}{T} + C_{ij} \ln T + D_{ij} + E_{ij} T + F_{ij} T^2 \tag{29}$$

$$\tau_{ij/ji} = \frac{A_{ij}}{T^2} + \frac{B_{ij}}{T} + C_{ij} \ln T + D_{ij} + E_{ij} T + F_{ij} T^2 \quad (30)$$

Table 5: Value for Eqs (30), (29) and $\alpha_{ij} = 0.3$ for each compound.

	Quantum corrected tc-PR g-WS MR					
	A_{ij} (K²)	B_{ij} (K)	C_{ij} (∅)	D_{ij} (∅)	E_{ij} (K⁻¹)	F_{ij} (K⁻²)
τ_{H_2/N_2}	0	2282.3	24.374	134.93	0	0
τ_{N_2/H_2}	0	319.44	6.6612	-32.359	0	0
k_{H_2/N_2}	0	-58.523	-0.98216	5.5434	0	0
$\tau_{H_2/CO}$	0	13123	268.20	-1227.9	-1.3823	0
τ_{CO/H_2}	0	-8670.7	-192.46	866.58	1.0721	0
$k_{H_2/CO}$	0	-723.21	-17.615	78.546	0.10293	0
τ_{H_2/CH_4}	0	-60.229	0	1.1400	0	0
τ_{CH_4/H_2}	0	70.832	0	0.027189	0	0
k_{H_2/CH_4}	0	0	0	2.8491	-0.030583	0.00010250
τ_{H_2/CO_2}	0	0	0	0.78679	0	0
τ_{CO_2/H_2}	0	0	0	102.95	0	0
k_{H_2/CO_2}	0	0	0	1.8057	0	0

Table 6: Value for Eqs (30), (29) and $\alpha_{ij} = 0.3$ for each compound.

	CAH g-WS MR					
	A_{ij} (K²)	B_{ij} (K)	C_{ij} (∅)	D_{ij} (∅)	E_{ij} (K⁻¹)	F_{ij} (K⁻²)
τ_{H_2/N_2}	-82245	6182.4	45.601	-263.94	0	0
τ_{N_2/H_2}	674209	-35144	-223.38	1313.8	0	0
k_{H_2/N_2}	-70258	3311.1	19.055	-113.33	0	0
$\tau_{H_2/CO}$	0	-37455	-1365.6	5373.9	15.887	-0.029922
τ_{CO/H_2}	0	97564	3224.1	-12948	-34.999	0.062551
$k_{H_2/CO}$	-3133681	262609	4093.9	-18709	-28.175	0.036151
τ_{H_2/CH_4}	0	102.25	0.97790	-4.9332	0	0
τ_{CH_4/H_2}	0	94.118	0.079272	-0.61237	0	0
k_{H_2/CH_4}	0	296.10	1.6997	-9.7835	0	0
τ_{H_2/CO_2}	0	0	0	0.79055	0	0
τ_{CO_2/H_2}	0	0	0	50.734	0	0
k_{H_2/CO_2}	0	0	0	1.7136	0	0

4.3. Results and discussion

4.3.a. Vapor-liquid equilibrium

Each mixture is characterized in Figures 4 and S7 in supplementary material section. The performance of the models is assessed using the BIAS and ARD functions, as defined in Eqs. (14) and (15), respectively. Here, (X_{exp}) represents the experimental vapor fraction (y_{exp}) of normal hydrogen, and (P_{exp}) the equilibrium pressure. The results are summarized in Table 7.

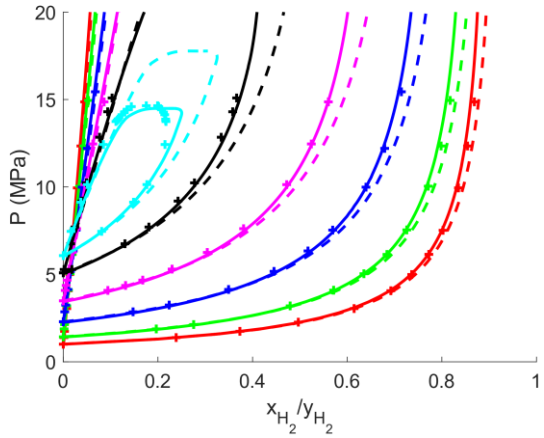

(a) H_2/CO_2 at temperatures are 233.15 (red), 243.15 (green), 258.15 (blue), 273.15 (pink), 288.15 (black), 295.65 K (cyan). Symbols are experimental data from Ref. [44].

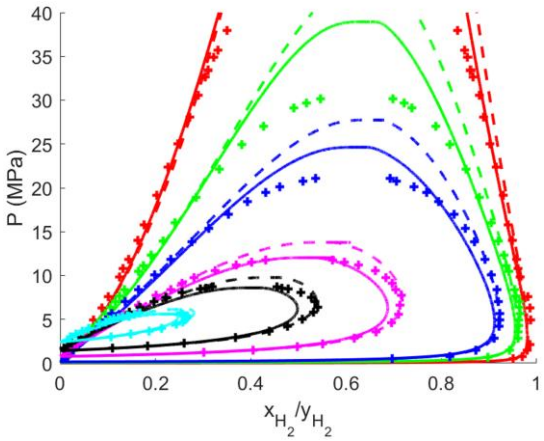

(b) H_2/CO at temperatures are 70 (red), 77.30 (green), 85 (blue), 105 (pink), 115 (black), 125 K (cyan). Symbols are experimental data from Ref. [46].

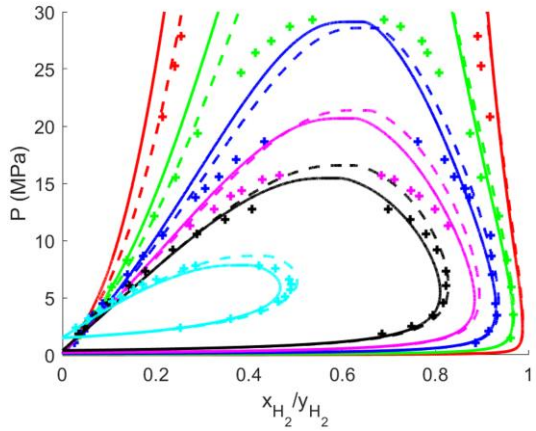

(c) H_2/N_2 at temperatures are 63.19 (red), 70.35 (green), 77.55 (blue), 83.67 (pink) 90.79 (black) and 110.30 K (cyan). Symbols are experimental data from Ref. [47].

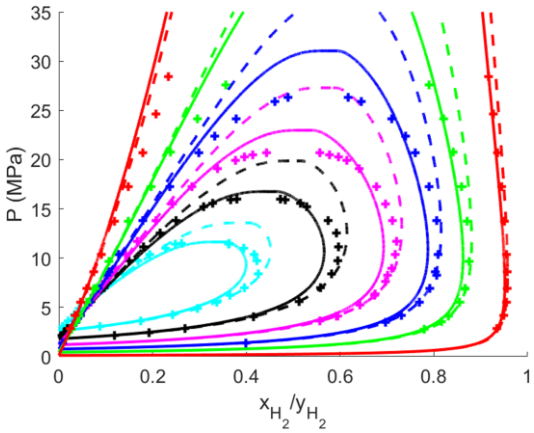

(d) H_2/CH_4 at temperatures are 113.14 (red), 133.14 (green), 143.48 (blue), 163.17 (pink), 173.25 (black) and 183.12 K (cyan). Symbols are experimental data from Ref. [48].

Figure 4: $P - xy$ binary system. Solid line: CAH EoS modeling with vdW MR, Dashed line: Quantum corrected tc-PR EoS modeling with vdW MR.

The H_2/CO_2 is better represented by the CAH EoS, with a binary interaction parameter (BIP) close to zero, compared to the quantum corrected tc-PR EoS. This is especially true for any isotherm, where the CAH EoS provides more accurate predictions. Figure 4a illustrates the modeling of bubble pressure, where the use of vdW MR shows good agreement with experimental data, particularly in vapor pressure modeling.

For the H_2/CO mixture, the CAH EoS exhibits less accuracy at high temperatures compared to the quantum corrected tc-PR EoS, with a maximum deviation of 17%. However, at lower temperatures, the CAH EoS performs comparably. Figure 4b demonstrates improved modelling of the critical region at 85 and $105\ \mathrm{K}$ using the CAH EoS.

For the H_2/N_2 mixture, higher BIP values are required for the CAH EoS compared to the quantum corrected tc-PR EoS. As shown in Figure 4c, the critical region is better represented with the CAH EoS, although the model's efficiency decreases at lower temperatures.

Table 7: Comparison of quantum corrected tc-PR vdW MR and CAH vdW MR evaluated with BIAS and ARD of pressure and vapor composition for hydrogen-containing binary mixture. References are based on experimental data.

H_2/CO_2														
EoS	**Quantum corrected tc-PR**							**CAH**						
T (K)	233.15	243.15	258.15	273.15	288.15	295.65	Avg	233.15	243.15	258.15	273.15	288.15	295.65	Avg
BIAS P	0.28	1.4	2.5	2.4	4.0	-2.0	1.4	-3.2	-1.8	-0.18	0.69	2.8	-0.70	-0.38
ARD P	0.74	1.5	2.5	3.2	4.0	5.0	2.8	3.3	2.9	1.0	2.1	2.8	3.5	2.6
BIAS y	-0.81	0.62	-0.25	1.5	2.3	-22	-3.1	-1.2	-0.046	-1.4	-0.19	4.2	-5.1	-0.62
ARD y	1.0	2.1	1.3	3.9	7.4	26	1.3	7.0	1.2	1.6	0.47	4.2	11	3.2
H_2/CO														
EoS	**Quantum corrected tc-PR**							**CAH**						
T (K)	70	77.3	85	105	115	125	Avg	70	77.3	85	105	115	125	Avg
BIAS P	-2.9	1.4	1.9	6.3	6.4	5.4	3.1	-9.2	-1.7	-3.2	1.3	2.8	3.7	-1.1
ARD P	11	11	7.9	6.3	6.4	5.4	8.0	17	11	9.0	5.1	4.0	3.8	8.3
BIAS y	0.092	0.99	2.2	4.7	6.5	10	-2.2	4.1	-0.87	-0.48	-0.36	-0.33	2.1	-0.36
ARD y	0.46	0.99	2.2	4.7	6.5	10	4.1	2.38	1.24	1.41	3.2	4.6	6.1	3.2
H_2/N_2														
EoS	**Quantum corrected tc-PR**							**CAH**						
T (K)	63.19	70.35	77.55	83.67	90.79	110.3	Avg	63.19	70.35	77.55	83.67	90.79	110.3	Avg
BIAS P	-56	-28	-8.3	-15	6.2	6.8	-16	-43	-15	-2.8	-13	5.7	5.2	-7.9
ARD P	56	29	13	15	8.8	6.8	21	-43	19	10	13	9.2	5.3	3.1
BIAS y	0.325	0.8	1.5	-0.85	1.8	4.4	-3.4	1.3	-1.9	-0.63	-6.0	-1.1	-1.8	-2.4
ARD y	0.35	0.79	1.6	0.93	1.9	4.9	1.7	3.4	2.0	0.83	6.0	1.4	4.0	2.9
H_2/CH_4														
EoS	**Quantum corrected tc-PR**							**CAH**						
T (K)	113.14	133.14	143.48	163.17	173.25	183.12	Avg	113.14	133.14	143.48	163.17	173.25	183.12	Avg

BIAS P	-4.3	-2.3	-6.1	-2.7	1.9	2.6	-2.7	-8.2	-0.82	-1.8	1.6	4.5	3.6	0.22
ARD P	8.4	5.2	8.0	4.8	4.0	2.9	11	6.1	4.7	5.1	2.7	4.5	3.6	5.0
BIAS y	-0.20	-1.0	-1.9	-3.7	-1.5	3.8	-1.7	0.86	1.5	2.9	4.2	7.1	12	4.6
ARD y	0.25	1.1	3.3	6.2	10	14	4.1	0.86	1.5	2.9	4.2	8.1	12	6.2

H_2/Ar

EoS	**Quantum corrected tc-PR**							**CAH**						
T (K)	83.09	95.77	104.11	111.46	122.73	134.91	Avg	83.09	95.77	104.11	111.46	122.73	134.91	Avg
BIAS P	1.7	11	12	10	11	9.3	9.1	9.3	-0.99	1.0	-0.94	2.3	3.4	3.3
ARD P	8.8	12	12	10	11	9.3	11	9.6	12	8.3	8.6	5.0	4.6	8.2
BIAS y	3.4	6.0	7.3	2.2	3.1	5.7	4.4	4.9	3.4	4.2	6.7	-3.3	-3.5	5.0
ARD y	4.2	6.3	7.7	3.0	3.7	9.2	5.0	5.3	3.9	4.8	7.0	3.5	6.3	5.7

H_2/He

EoS	**Quantum corrected tc-PR**							**CAH**						
T (K)	15.4	20.4	23.0	26.0	29.0	31.0	Avg	15.4	20.4	23.0	26.0	29.0	31.0	Avg
BIAS P	49	18	21	15	5.7	2.8	19	-15	-2.8	7.4	9.2	5.1	4.3	1.4
ARD P	49	39	21	15	8.0	5.1	23	15	6.9	9.6	10	8.0	5.4	9.2
BIAS y	1.2	2.7	3.9	4.9	2.4	2.8	3.0	-0.53	-2.1	0.17	2.4	2.8	7.8	1.8
ARD y	1.2	3.8	3.9	6.0	8.9	11	5.8	0.53	3.1	1.4	4.4	10	11	5.1

H_2/H_2O

EoS	**Quantum corrected tc-PR**							**CAH**						
T (K)	310.89	366.46	422.00	477.55	573.11	588.67	Avg	310.89	366.46	422.00	477.55	573.11	588.67	Avg
BIAS P	3.6	5.2	-1.2	-6.7	3.6	-10	-0.92	-10	7.7	4.5	-5.2	1.1	-12	-2.3
ARD P	3.6	5.8	1.3	6.7	19	10	7.7	10	7.9	4.5	5.3	20	12	10
BIAS y	-0.073	-0.26	-0.20	-2.9	7.6	17	3.5	-0.038	0.56	1.2	-0.96	5.2	8.2	2.4
ARD y	0.079	0.36	0.20	3.2	20	17	6.8	0.051	0.56	1.2	2.2	20	8.2	5.4

In the case of the H_2/CH_4 mixture, the CAH EoS model shows a maximum deviation of 12% and requires higher BIP values than the quantum corrected tc-PR EoS. Figure 4d indicates that the CAH EoS more accurately represents the vapor-liquid equilibrium (VLE) near the critical point of the mixture, with a pressure deviation of $4\ \mathrm{MPa}$ at $163.17\ \mathrm{K}$.

For the H_2/Ar mixture, the CAH EoS demonstrates poor representation of vapor pressure at low temperatures. However, it is more accurate around the critical point at 95.77, 104.11, and 111.46 K, as depicted in Figure S7a in supplementary material section. The vapor pressure of this mixture is adequately represented by both the quantum corrected tc-PR and CAH EoS models.

The H_2/He mixture, composed of two cryogenic compounds, requires special consideration due to the quantum effects of these components. The inclusion of a temperature dependence on the BIP allows the CAH EoS to outperform the quantum corrected tc-PR EoS. While the critical region at $29\ \mathrm{K}$ is less accurately modeled with the CAH EoS, as shown in Figure S7b in supplementary material section, it remains effective across other isotherms with a maximum deviation of 15%.

The H_2/H_2O mixture is challenging due to the polarity of the water molecule, which is poorly represented by cubic equations of state. The addition of a BRP and temperature dependence on the BIP improves the accuracy and stability of the model, achieving a maximum deviation of 20%, as shown in Figure S7c in supplementary material section. These difficulties can be overcome by using phase-specific binary interaction coefficients [49] [50], but the model becomes inconsistent in the region of the mixture critical point.

Overall, the CAH EoS with vdW MR provides a superior representation of VLE in binary systems compared to the quantum corrected tc-PR EoS with vdW MR, especially around the critical point. This model was initially designed to improve the prediction of equilibrium pressures near the critical region. Minor adjustments for non-quantum and non-polar mixtures were made to enhance the efficacy of the CAH EoS model. For more complex mixtures, incorporating temperature dependencies and constants is essential, though these modifications remain relatively straightforward.

The use of mixing rules significantly enhances modelling accuracy near the critical region. Moreover, temperature dependencies further improve the model's precision. The H_2/CO_2 allows for a comparison between temperature-dependent mixing rules, demonstrating that the g-WS MR

mixing rule corrects the shortcomings of the vdW MR. The accuracy gain is more pronounced with the quantum corrected tc-PR EoS than with the CAH EoS, indicating that the CAH EoS better captures molecular interactions and is less reliant on the choice of mixing rules.

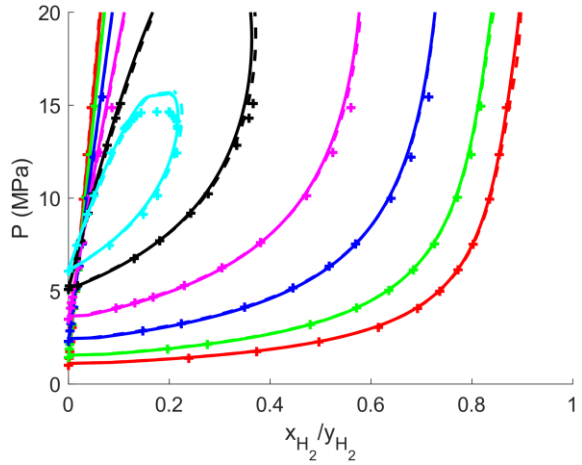

(a) H_2/CO_2 at temperatures are 233.15 (red), 243.15 (green), 258.15 (blue), 273.15 (pink), 288.15 (black), 295.65 K (cyan). Symbols are experimental data from Ref. [44].

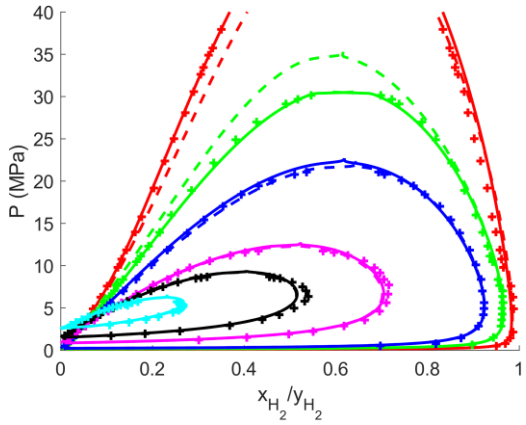

(b) H_2/CO at temperatures are 70 (red), 77.30 (green), 85 (blue), 105 (pink), 115 (black), 125 K (cyan). Symbols are experimental data from Ref. [46].

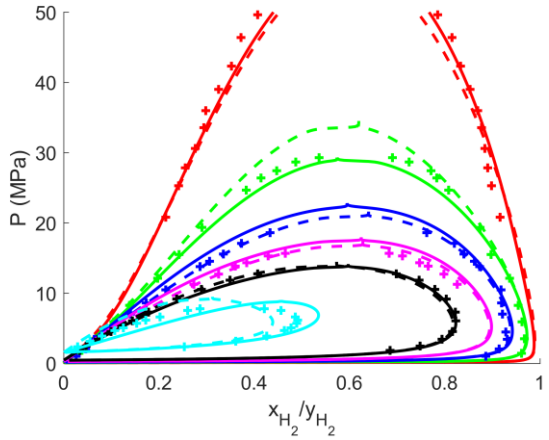

(c) H_2/N_2 at temperatures are 63.19 (red), 70.35 (green), 77.55 (blue), 83.67 (pink) 90.79 (black) and 110.30 K (cyan). Symbols are experimental data from Ref. [47].

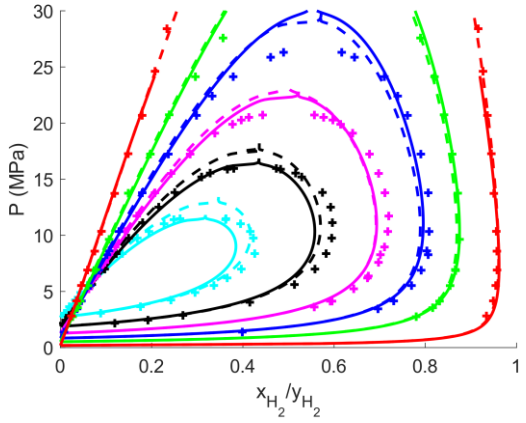

(d) H_2/CH_4 at temperatures are 113.14 (red), 133.14 (green), 143.48 (blue), 163.17 (pink), 173.25 (black) and 183.12 K (cyan). Symbols are experimental data from Ref. [48].

Figure 5: $P - xy$ binary system. Solid line: CAH EoS modeling with g-WS MR mixing rules, Dashed line: Quantum corrected tc-PR EoS modeling with g-WS MR.

The results obtained with g-WS MR are shown in Figure 5 and the BIAS and ARD values are listed in Table 8. The predictions using the g-WS MR with temperature dependence of the BIP are more

accurate in comparison to the predictions using the vdW-MR. The H_2/CO_2 mixture is accurately modelled, the critical region of this mixture at $295.65\ K$ is slightly overestimated. The critical zone of the binary mixtures H_2/CO and H_2/N_2 are better predicted considering the g-WS MR associated with the CAH EoS instead the quantum corrected tc-PR EoS. Considering binary H_2/CH_4 system, at the lowest temperatures the prediction with the CAH g-WS MR overestimates critical region. Otherwise, at the highest temperature with the same model we observe on overestimation of the critical region. All the VLE of the studied mixture are accurately predicted with g-vdW MR. Otherwise, combining the g-WS MR with temperature dependence of the BIP leads to the best prediction of the VLE for each studied mixture. Also, using CAH EoS instead quantum corrected tc-PR EoS increases the prediction accuracy around the critical region whatever the mixture rule used.

Table 8: Comparison of quantum corrected tc-PR g-WS MR and CAH g-WS MR evaluated with BIAS and ARD of pressure and vapor composition for hydrogen-containing binary mixture. References are based on experimental data.

H_2/CO_2														
EoS	**Quantum corrected tc-PR**							**CAH**						
T (K)	233.15	243.15	258.15	273.15	288.15	295.65	Avg	233.15	243.15	258.15	273.15	288.15	295.65	Avg
BIAS x	1.1	2.3	5.2	4.3	-3.6	-0.80	1.4	-1.0	1.1	5.4	5.5	-2.6	3.2	1.9
ARD x	2.3	3.9	5.2	4.3	3.6	6.5	4.3	2.5	3.9	5.4	5.5	3.6	5.5	4.4
BIAS y	-0.30	-0.42	-0.63	-0.52	1.2	-3.6	-0.71	-0.31	-0.95	-1.8	-2.4	-1.2	-0.56	-1.2
ARD y	0.41	0.69	1.4	1.4	1.5	5.4	1.8	0.49	1.3	2.6	3.6	4.5	3.6	2.7
H_2/CO														
EoS	**Quantum corrected tc-PR**							**CAH**						
T (K)	70	77.30	85	105	115	125	Avg	70	77.30	85	105	115	125	Avg
BIAS x	-6.7	11	0.32	0.34	3.8	0.12	1.5	1.2	-0.91	3.4	1.2	0.083	0.48	0.91
ARD x	9.3	11	3.1	2.3	3.8	2.8	5.4	2.1	2.8	3.4	2.2	2.1	2.8	2.6
BIAS y	1.2	-1.0	0.31	1.3	1.4	1.1	0.74	-0.42	0.18	0.21	0.65	1.0	1.7	0.75
ARD y	2.3	1.1	0.64	1.7	2.4	2.9	1.8	1.2	0.68	0.84	1.5	2.5	3.2	1.7
H_2/N_2														
EoS	**Quantum corrected tc-PR**							**CAH**						
T (K)	63.19	70.35	77.55	83.67	90.79	110.30	Avg	63.19	70.35	77.55	83.67	90.79	110.30	Avg
BIAS x	-7.0	9.3	0.53	-2.7	1.4	34	6.0	-5.0	-4.7	11	6.7	-7.0	-41	-6.7
ARD x	7.3	9.3	5.4	2.7	1.5	34	10	5.3	6.5	11	6.7	7.0	41	13
BIAS y	3.0	-1.6	-0.033	-3.7	0.52	7.4	0.92	0.48	3.1	-1.0	-6.1	-0.5	-10	-2.4
ARD y	4.1	1.6	0.82	3.7	2.1	7.4	3.3	1.8	3.5	1.3	6.1	1.5	10	4.1
H_2/CH_4														
EoS	**Quantum corrected tc-PR**							**CAH**						
T (K)	113.14	133.14	143.48	153.21	163.17	173.25	Avg	113.14	133.14	143.48	153.21	163.17	173.25	Avg

BIAS x	1.8	2.7	5.1	4.2	5.7	5.0	4.1	2.1	2.4	4.1	4.6	3.1	12	4.7
ARD x	-0.3	2.1	4.6	3.6	5.7	1.1	2.8	-0.35	-0.037	2.1	-0.66	-2.0	-12	-2.1
BIAS y	0.39	0.46	2.8	3.0	3.6	4.1	2.4	0.65	0.26	2.5	2.9	4.4	7.9	3.1
ARD y	-0.26	0.44	1.3	1.6	1.1	-0.15	0.68	-0.068	-0.24	0.048	1.6	4.4	7.9	2.3

4.3.b. Density

The accuracy of density representation of the model is assessed through the BIAS and ARD functions, as defined by Eqs (14) and (15), respectively. Here, (X) denotes the experimental density of the mixture (ρ_{exp}). The results for vdW MR and g-WS MR are summarized in Tables 9, 10 and 11. The BIP and BRP used are the same as those adjusted based on VLE data and presented in Table 4.

Table 9: Performance comparison between quantum corrected tc-PR EoS, CAH EoS vdW MR and quantum corrected tc-PR EoS, CAH EoS g-WS MR for H_2/N_2 mixture [51].

EoS		Quantum corrected tc-PR vdW MR		CAH vdW MR		Quantum corrected tc-PR g-WS MR		CAH g-WS MR	
x_{H2}	T (K)	BIAS ρ	ARD ρ	BIAS ρ	ARD ρ	BIAS ρ	ARD ρ	BIAS ρ	ARD ρ
0.0532	397.9	1.2	1.2	-2.8	2.8	1.5	1.5	-1.7	1.8
	373.2	0.94	1.1	-3.0	3.0	0.69	1	-1.6	1.8
	348.4	1.1	1.1	-2.7	2.7	0.84	1.2	-1.6	1.6
	323.6	1.0	1.2	-2.9	2.9	0.46	1.4	-1.5	1.6
	298.4	0.66	1.0	-2.9	2.9	0.68	1.5	-2.0	2.0
	278.2	0.82	1.1	-2.2	2.2	0.78	1.6	-1.2	1.4
	Avg	0.95	1.1	-2.8	2.8	0.83	1.4	-1.6	1.7
0.0858	397.9	1.3	1.3	-3.0	3.0	1.8	1.8	-0.25	1.7
	373.2	1.3	1.3	-2.8	2.8	0.94	1.5	-0.63	1.6
	348.4	0.94	1.1	-2.8	2.8	0.43	1.5	-1.0	1.7
	323.6	0.65	1.0	-3.2	3.2	0.51	1.7	-1.6	2.2
	298.4	0.51	0.89	-2.2	2.2	-0.65	1.7	-0.3	1.7
	278.2	0.94	1.2	-2.2	2.2	1.1	2.0	-0.73	1.5
	Avg	0.94	1.1	-2.7	2.7	0.7	1.7	-0.75	1.7
0.2031	397.9	1.5	1.5	-2.7	2.7	-0.15	1.8	7.3	7.3
	372.7	1.1	1.1	-2.6	2.6	-2.9	4.5	3.9	4.4
	348.4	1.0	1.0	-2.7	2.7	-3.0	4.8	3.1	3.9
	323.4	0.62	0.66	-2.2	2.2	-4.3	5.8	2.9	4.0
	298.2	0.37	0.51	-2.4	2.4	-1.3	3.9	1.0	3.0
	278.1	0.45	0.57	-2.3	2.3	-0.89	3.5	1.4	3.1
	Avg	-0.36	0.36	-1.7	1.7	-2.4	2.4	-1.1	1.5

Table 10: Performance comparison between quantum corrected tc-PR EoS, CAH EoS vdW MR and quantum corrected tc-PR EoS, CAH EoS g-WS MR for H_2/CH_4 mixture [52].

EoS		Quantum corrected tc-PR vdW MR		CAH vdW MR		Quantum corrected tc-PR g-WS MR		CAH g-WS MR	
x_{H2}	T (K)	BIAS ρ	ARD ρ	BIAS ρ	ARD ρ	BIAS ρ	ARD ρ	BIAS ρ	ARD ρ
0.0532	397.9	1.2	1.2	-2.8	2.8	1.5	1.5	-1.7	1.8
	373.2	0.94	1.1	-3.0	3.0	0.69	1.0	-1.6	1.8
	348.4	1.1	1.1	-2.7	2.7	0.84	1.2	-1.6	1.6
	323.6	1.0	1.2	-2.9	2.9	0.46	1.4	-1.5	1.6
	298.4	0.66	1.0	-2.9	2.9	0.68	1.5	-2.0	2.0
	278.2	0.82	1.1	-2.2	2.2	0.78	1.6	-1.2	1.4
	Avg	0.95	1.1	-2.8	2.8	0.83	1.4	-1.6	1.7
0.0858	397.9	1.3	1.3	-3.0	3.0	1.8	1.8	-0.25	1.7
	373.2	1.3	1.3	-2.8	2.8	0.94	1.5	-0.63	1.6
	348.4	0.94	1.1	-2.8	2.8	0.43	1.5	-1.0	1.7
	323.6	0.65	1.0	-3.2	3.2	0.51	1.7	-1.6	2.2
	298.4	0.51	0.89	-2.2	2.2	-0.65	1.7	-0.3	1.7
	278.2	0.94	1.2	-2.2	2.2	1.1	2.0	-0.73	1.5
	Avg	0.94	1.1	-2.7	2.7	0.70	1.7	-0.75	1.7
0.2031	397.9	1.5	1.5	-2.7	2.7	-0.15	1.8	7.3	7.3
	372.7	1.1	1.1	-2.6	2.6	-2.9	4.5	3.9	4.4
	348.4	1.0	1.0	-2.7	2.7	-3.0	4.8	3.1	3.9
	323.4	0.62	0.66	-2.2	2.2	-4.3	5.8	2.9	4.0
	298.2	0.37	0.51	-2.4	2.4	-1.3	3.9	1.0	3.0
	278.1	0.45	0.57	-2.3	2.3	-0.89	3.5	1.4	3.1
	Avg	0.76	0.81	-2.4	2.4	-2.1	4.0	3.3	4.3

Table 11: Performance comparison between quantum corrected tc-PR EoS, CAH EoS vdW MR and quantum corrected tc-PR EoS, CAH EoS g-WS MR H_2/CO_2 mixture [53],[54].

EoS		Quantum corrected tc-PR vdW MR		CAH vdW MR		Quantum corrected tc-PR g-WS MR		CAH g-WS MR	
x_{H2}	T (K)	BIAS ρ	ARD ρ	BIAS ρ	ARD ρ	BIAS ρ	ARD ρ	BIAS ρ	ARD ρ
0.0536	273.15	-0.51	0.51	-1.9	1.9	-0.61	0.61	-1.9	1.9
	293.15	-1.0	1.0	-3.0	3.0	-1.1	1.1	-3.0	3.0
	323.15	-1.1	1.1	-3.2	3.2	-1.2	1.2	-3.2	3.2
	Avg	-0.92	0.92	-1.6	1.6	-0.88	0.88	-2.7	2.7
0.8633	323.15	-0.68	0.68	-1.5	1.5	-1.2	1.2	-1.3	1.3
	348.15	-0.77	0.77	-1.5	1.5	-1.3	1.3	-1.7	1.7
	373.15	-0.83	0.83	-1.5	1.5	-1.3	1.3	-1.8	1.8
	398.15	-0.83	0.83	-1.4	1.4	-1.3	1.3	-1.7	1.7
	423.15	-0.83	0.83	-1.3	1.3	-1.3	1.3	-1.7	1.7
	Avg	-1.0	1.0	-1.5	1.5	-0.79	0.79	-1.4	1.4
0.2341	323.15	-1.5	1.5	-3.1	3.1	-1.8	1.8	-3.1	3.1
	348.15	-1.1	1.1	-2.6	2.6	-1.5	1.5	-2.7	2.7
	373.15	-0.93	0.93	-2.2	2.2	-1.2	1.2	-2.3	2.3
	398.15	-0.77	0.77	-2.0	2.0	-0.97	0.97	-2.0	2.0
	423.15	-0.67	0.67	-1.9	1.9	-0.80	0.80	-1.9	1.9
	Avg	-1.2	1.2	-2.5	2.5	-1.0	1.0	-2.3	2.3

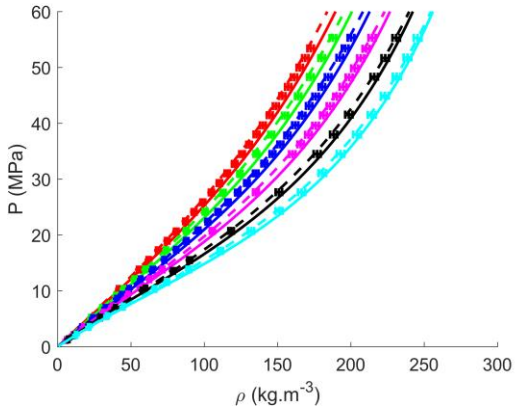

(a) H_2/CH_4 mixture. Composition: x_{H2} = 0.2031. Temperatures: 397.9 (red), 372.7 (green), 348.4 (blue), 323.6 (pink), 298.2 (black) and 278.1 K (cyan). Symbols are experimental data from Ref. [52].

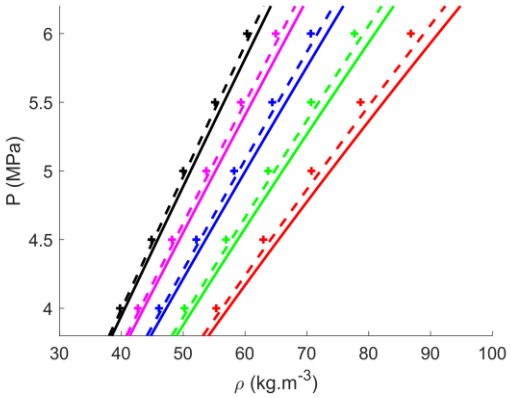

(b) H_2/CO_2 mixture. Composition: x_{H2} = 0.2341. Temperatures: 323.15 (red), 348.15 (green), 373.15 (blue), 398.15 (pink), 423.15 K (black). Symbols are experimental data from Ref. [53],[54]

Figure 6: Pressure of normal hydrogen binary mixture as a function of densities at different temperatures and compositions. Solid line: CAH EoS modeling with vdW MR, Dashed line: Quantum corrected tc-PR EoS modeling with vdW MR.

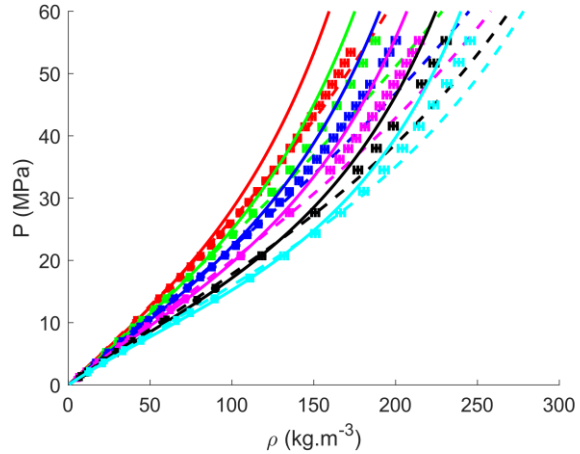

(a) H_2/CH_4 mixture. Composition: x_{H2} = 0.2031. Temperatures: 397.9 (red), 372.7 (green), 348.4 (blue), 323.6 (pink), 298.2 (black) and 278.1 K (cyan). Symbols are experimental data from Ref. [52].

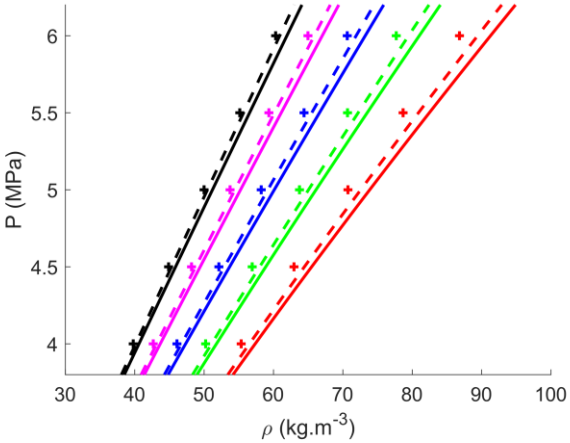

(b) H_2/CO_2 mixture. Composition: x_{H2} = 0.2341. Temperatures: 323.15 (red), 348.15 (green), 373.15 (blue), 398.15 (pink), 423.15 K (black). Symbols are experimental data from Ref. [53],[54]

Figure 7: Pressure of normal hydrogen binary mixture as a function of densities at different temperatures and compositions. Solid line: CAH EoS modelling with g-WS MR, Dashed line: Quantum corrected tc-PR EoS modelling with g-WS MR.

Figure 6 shows that the density of the H_2/CH_4 and H_2/CO_2 binary mixtures are better represented with the quantum corrected tc-PR EoS than by the CAH EoS involving with the vdW MR. In Figure 7, we can observe that application of g-WS MR lead to worst prediction for the H_2/CH_4 binary system particularly in the domain of temperature and pressure different from those considered for the parameters adjustment. For the binary H_2/CO_2 system, the prediction by using g-WS MR are less accurate than those from the vdW MR in comparison of the experimental data. For the H_2/N_2 binary system, Figures 8 and 9 show that, with the vdW MR the CAH EoS are less accurate than those with the quantum corrected tc-PR EoS in comparison to the experimental data. Changing the vdW MR by the g-WS MR do not improve significantly the density predictions.

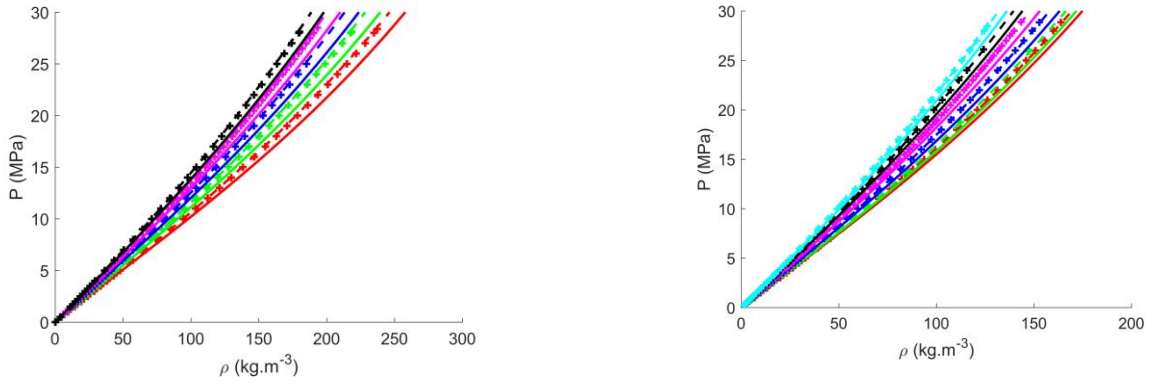

(a) Composition: $x_{H2} = 0.2499$. Temperatures: 270 (red), 290 (green), 310 (blue), 330 (pink), 350 K (black).

(b) Composition: $x_{H2} = 0.5002$. Temperatures: 270 (red), 275 (green), 290 (blue), 310 (pink), 350 K (cyan).

Figure 8: Pressure of binary mixture H_2/N_2 as a function of densities at different temperatures and compositions. Solid line: CAH EoS modeling with vdW MR, Dashed line: Quantum corrected tc-PR EoS modeling with vdW MR. Symbols are experimental data from Ref. [51].

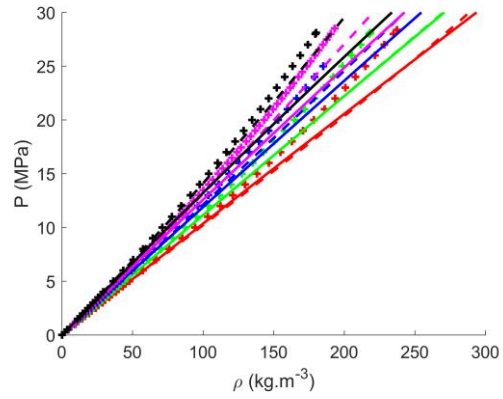

(a) Composition: x_{H2} = 0.2499. Temperatures: 270 (red), 290 (green), 310 (blue), 330 (pink), 350 K (black).

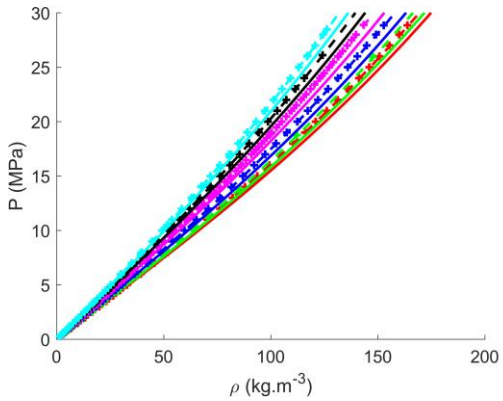

(b) Composition: x_{H2} = 0.5002. Temperatures: 270 (red), 275 (green), 290 (blue), 310 (pink), 350 K (cyan).

Figure 9: Pressure of binary mixture H_2/N_2 as a function of densities at different temperatures and compositions. Solid line: CAH EoS modeling with g-WS MR, Dashed line: Quantum corrected tc-PR EoS modelling with g-WS MR. Symbols are experimental data from Ref. [51].

Nevertheless, considering the fact that EoS theory is based on the mean field theory, it is possible to extrapolate phase equilibrium and thermodynamic property predictions outside the range of temperature pressure and composition considered in parameter adjustments [24][55]. The prediction capability involving the g-WS MR depends strongly on the quality of the experimental data used for BIP adjustments. Using suspicious VLE data can lead to a false prediction of density. It is not the case using vdW MR as this mixture rule required only one BIP less sensitive to the quality of the data. The relevance of the mixing rules proposed in this article can be assessed in more detail by considering predictions of the speed of sound and heat capacity at constant pressure. A recent paper by Lozano-Martin et al. [56] reports speed of sound measurements in the binary mixture H_2/N_2 while van Itterbeek et al. [57] provides measurements for the binary mixtures H_2/CH_4 and H_2/CO. On the basis of these studies, a complementary investigation must be realized to validate the mixing rules capability used to predict the speed of sound of H_2/N_2 binary mixtures.

5. Conclusion

Hydrogen is an energy carrier that is gradually being developed on an industrial scale. The need to develop reliable thermodynamic models is central to the development of efficient production processes [58][59]. The well-known models such as GERG-2008 and PC-SAFT EoS show comparable results with

the cubic EoS models [60]. However, if the GERG-2008 and the PC-SAFT EoSs have to be used with a new binary system involving hydrogen, it will require numerous experimental data for the adjustment of the BIP, which is not the case with cubic EoSs due to their simplicity [61]. Thermodynamic models are primarily used in macroscopic simulation software, and the calculation time should be minimized as much as possible to facilitate their application.

The CAH EoS strikes a balance between precision in thermodynamic modelling and simplicity. Its adaptation for modelling normal hydrogen and its "quantum swelling phenomenon" extends its applicability while maintaining minimal corrections within its performance range. The CAH EoS is comparable to or even exceeds the quantum corrected tc-PR EoS model in accuracy for various thermodynamic properties used in industrial applications, while maintaining a reasonable number of numerical parameters. This feature notably mitigates the impact of volume translation effects associated with the quantum corrected tc-PR EoS.

For binary mixtures, the CAH EoS model demonstrates superior accuracy around the critical region compared to the quantum corrected tc-PR EoS. The vdW MR is adequate for modelling these mixtures accurately. However, for more complex mixtures, temperature-dependent BIP and the inclusion of a BRP are necessary to achieve correct results. Although densities using the vdW MR show slightly lower precision than those with the quantum corrected tc-PR EoS, the CAH EoS maintains consistent accuracy across all compositions and temperatures.

The g-WS MR requires temperature dependence to model mixtures accurately. Nevertheless, this mixing rule is more unstable during optimization and significantly impacts the efficiency of density modelling for mixtures. These EoS form the basis for process design and must be both precise and reasonably complex. When using g-WS MR, constraining the model to a few experimental density points while optimizing for VLE could help avoid these multiple root problems. They facilitate the modelling of binary mixtures commonly encountered in industrial applications and can be easily extended to multiconstituant mixtures.

6. **Acknowledgements**

We would like to thank the research initiation program at Institution Mines Telecom Mines Albi for providing the equipment needed to carry out this project.

7. **Supplementary materials**

Supplementary data to this article can be found online at Supplementary material

References

1. Hanto, J., Herpich, P., Löffler, K., Hainsch, K., Moskalenko, N. & Schmidt, S. Assessing the implications of hydrogen blending on the European energy system towards 2050. en. *Advances in Applied Energy* 13, 100161. doi:10.1016/j.adapen.2023.100161 (february 2024).
2. Salvi, B. & Subramanian, K. Sustainable development of road transportation sector using hydrogen energy system. en. *Renewable and Sustainable Energy Reviews* 51, 1132–1155. doi:10.1016/j.rser.2015.07.030 (november 2015).
3. Sellami, M. & Loudiyi, K. Electrolytes behavior during hydrogen production by solar energy. en. *Renewable and Sustainable Energy Reviews* 70, 1331–1335. doi:10.1016/ j.rser.2016.12.034 (april 2017).
4. Blanquet, E. & Williams, P. T. Biomass pyrolysis coupled with non-thermal plasma/catalysis for hydrogen production: Influence of biomass components and catalyst properties. en. *Journal of Analytical and Applied Pyrolysis* 159, 105325. doi:10.1016/j.jaap.2021. 105325 (october 2021).
5. Alhamed, H., Behar, O., Saxena, S., Angikath, F., Nagaraja, S., Yousry, A., Das, R., Altmann, T., Dally, B. & Sarathy, S. M. From methane to hydrogen: A comprehensive review to assess the efficiency and potential of turquoise hydrogen technologies. *International Journal of Hydrogen Energy* 68, 635–662. doi:10.1016/j.ijhydene.2024.04.231 (may 2024).
6. Sánchez-Bastardo, N., Schlögl, R. & Ruland, H. Methane Pyrolysis for Zero-Emission Hydrogen Production: A Potential Bridge Technology from Fossil Fuels to a Renewable and Sustainable Hydrogen Economy. en. *Industrial & Engineering Chemistry Research* 60, 11855–11881. doi:10.1021/acs.iecr.1c01679 (august 2021).
7. Moradi, R. & Groth, K. M. Hydrogen storage and delivery: Review of the state of the art technologies and risk and reliability analysis. en. *International Journal of Hydrogen Energy* 44, 12254–12269. doi:10.1016/j.ijhydene.2019.03.041 (may 2019).
8. Yang, J., Li, Y. & Tan, H. An energy-saving hydrogen liquefaction process with efficient utilization of liquefied natural gas cold energy. en. *International Journal of Hydrogen Energy* 49, 1482–1496. doi:10.1016/j.ijhydene.2023.09.246 (january 2024).
9. Wilhelmsen, Ø., Berstad, D., Aasen, A., Nekså, P. & Skaugen, G. Reducing the exergy destruction in the cryogenic heat exchangers of hydrogen liquefaction processes. en. *International Journal of Hydrogen Energy* 43, 5033–5047. doi:10.1016/j.ijhydene. 2018.01.094 (march 2018).
10. Giddey, S., Badwal, S. P. S., Munnings, C. & Dolan, M. Ammonia as a Renewable Energy Transportation Media. en. *ACS Sustainable Chemistry & Engineering* 5, 10231–10239. doi:10.1021/acssuschemeng.7b02219 (november 2017).
11. Petrescu, R. V., Aversa, R., Akash, B., Bucinell, R., Corchado, J., Berto, F., Mirsayar, M., Apicella, A. & Petrescu, F. I. T. Modern Propulsions for Aerospace-A Review. en. *Journal of Aircraft and Spacecraft Technology* 1ʾ 1–8. doi:10.3844/jastsp.2017.1.8 (january 2017).

12. Murphy, A. B. Transport Coefficients of Hydrogen and Argon–Hydrogen Plasmas. en. *Plasma Chemistry and Plasma Processing* 20, 279–297. doi:10.1023/A:1007099926249 (2000).

13. Mazloomi, K. & Gomes, C. Hydrogen as an energy carrier: Prospects and challenges. en. *Renewable and Sustainable Energy Reviews* 16, 3024–3033. doi:10.1016/j.rser. 2012.02.028 (june 2012).

14. Ramachandran, R. & Menon, R. K. An overview of industrial uses of hydrogen. *International Journal of Hydrogen Energy* 23, 593–598. doi:10.1016/S0360-3199(97)00112-2 (july 1998).

15. Wei, C., Jafari Raad, S. M., Leonenko, Y. & Hassanzadeh, H. Correlations for prediction of hydrogen gas viscosity and density for production, transportation, storage, and utilization applications. *International Journal of Hydrogen Energy* 48, 34930–34944. doi:10.1016/j.ijhydene.2023.05.202 (november 2023).

16. Aasen, A., Hammer, M., Lasala, S., Jaubert, J.-N. & Wilhelmsen, Ø. Accurate quantumcorrected cubic equations of state for helium, neon, hydrogen, deuterium and their mixtures. en. *Fluid Phase Equilibria* 524, 112790. doi:10.1016/j.fluid.2020.112790 (december 2020).

17. Peng, D.-Y. & Robinson, D. B. A New Two-Constant Equation of State. en. *Industrial & Engineering Chemistry Fundamentals* 15, 59–64. doi:10.1021/i160057a011 (february 1976).

18. Liu, B., Liu, X., Lu, C., Godbole, A., Michal, G. & Teng, L. Decompression of hydrogen—natural gas mixtures in high-pressure pipelines: CFD modelling using different equations of state. *International Journal of Hydrogen Energy* 44, 7428–7437. doi:10.1016/j. ijhydene.2019.01.221 (march 2019).

19. Liu, X., Michal, G., Godbole, A. & Lu, C. Decompression modelling of natural gashydrogen mixtures using the Peng-Robinson equation of state. *International Journal of Hydrogen Energy* 46, 15793–15806. doi:10.1016/j.ijhydene.2021.02.129 (april 2021).

20. Jaubert, J.-N., Privat, R., Le Guennec, Y. & Coniglio, L. Note on the properties altered by application of a Péneloux–type volume translation to an equation of state. en. *Fluid Phase Equilibria* 419, 88–95. doi:10.1016/j.fluid.2016.03.012 (july 2016).

21. Quinzio, M. J., Rodriguez-Reartes, S. B. & Cismondi-Duarte, M. Phase behavior and type of non-ideality in n-alkanes mixtures predicted from equations of state: The role of a third parameter. *Fluid Phase Equilibria* 577, 113963. doi:https://doi.org/10.1016/j.fluid.2023.113963 (2024).

22. Piña-Martinez, A., Privat, R., Lasala, S., Soave, G. & Jaubert, J.-N. Search for the optimal expression of the volumetric dependence of the attractive contribution in cubic equations of state. en. *Fluid Phase Equilibria* 522, 112750. doi:10.1016/j.fluid.2020.112750 (november 2020).

23. Coquelet, C., El Abbadi, J. & Houriez, C. Prediction of thermodynamic properties of refrigerant fluids with a new three-parameter cubic equation of state. en. *International Journal of Refrigeration* 69, 418–436. doi:10.1016/j.ijrefrig.2016.05.017 (september 2016).

24. Privat, R. & Jaubert, J.-N. The state of the art of cubic equations of state with temperature-dependent binary interaction coefficients: From correlation to prediction. en. *Fluid Phase Equilibria* 567, 113697. doi:10.1016/j.fluid.2022.113697 (april 2023).

25. Feynman, R. P., Hibbs, A. R. & Styer, D. F. *Quantum mechanics and path integrals* (Courier Corporation, 2010).

26. Han, S. P. A globally convergent method for nonlinear programming. en. *Journal of Optimization Theory and Applications* 22, 297–309. doi:10.1007/BF00932858 (1977).

27. *Mathematical Programming The State of the Art* en (editors Bachem, A., Korte, B. & Grötschel, M.) doi:10.1007/978-3-642-68874-4 (Springer Berlin Heidelberg, Berlin, Heidelberg, 1983).

28. *Numerical analysis. 7: Proceedings of the biennial conference held at Dundee, June 28 July 1, 1977 / [7th Dundee Biennial Conference on Numerical Analysis.] Ed. by G. A. Watson* en (editor Watson, G. A.) *Lecture notes in mathematics* 630. Meeting Name: Dundee Conference on Numerical Analysis (Springer, Berlin Heidelberg, 1978).

29. Philip E. Gill, Walter Murray, Margaret H. Wright-Practical. *Practical Optimization* (Harcourt Barce and Company, 1982).

30. Leachman, J. W., Jacobsen, R. T., Penoncello, S. G. & Lemmon, E. W. Fundamental Equations of State for Parahydrogen, Normal Hydrogen, and Orthohydrogen. en. *Journal of Physical and Chemical Reference Data* 38, 721–748. doi:10.1063/1.3160306 (september 2009).

31. Vega, D. O., Hall, K., Holste, J., Harvey, A. H. & Lemmon, E. W. An equation ofstate for the thermodynamic properties of helium.Technical Report No. NISTIR 8474(2023).

32. Span, R. & Wagner, W. A New Equation of State for Carbon Dioxide Covering the Fluid Region from the Triple-Point Temperature to 1100 K at Pressures up to 800 MPa. en. *Journal of Physical and Chemical Reference Data* 25, 1509–1596. doi:10.1063/1. 555991 (november 1996).

33. Lemmon, E. W. & Span, R. Short Fundamental Equations of State for 20 Industrial Fluids. en. *Journal of Chemical & Engineering Data* 51, 785–850. doi:10.1021/je050186n (may 2006).

34. Tegeler, C., Span, R. & Wagner, W. A New Equation of State for Argon Covering the Fluid Region for Temperatures From the Melting Line to 700 K at Pressures up to 1000 MPa. en. *Journal of Physical and Chemical Reference Data* 28, 779–850. doi:10.1063/ 1.556037 (may 1999).

35. Span, R., Lemmon, E. W., Jacobsen, R. T., Wagner, W. & Yokozeki, A. A Reference Equation of State for the Thermodynamic Properties of Nitrogen for Temperatures from 63.151 to 1000 K and Pressures to 2200 MPa. en. *Journal of Physical and Chemical Reference Data* 29, 1361–1433. doi:10.1063/1.1349047 (november 2000).

36. Wagner, W. & Pruß, A. The IAPWS Formulation 1995 for the Thermodynamic Properties of Ordinary Water Substance for General and Scientific Use. en. *Journal of Physical and Chemical Reference Data* 31, 387–535. doi:10.1063/1.1461829 (june 2002).

37. Setzmann, U. & Wagner, W. A New Equation of State and Tables of Thermodynamic Properties for Methane Covering the Range from the Melting Line to 625 K at Pressures up to 100 MPa. en. *Journal of Physical and Chemical Reference Data* 20, 1061–1155. doi:10.1063/1.555898 (november 1991).

38. Le Guennec, Y., Privat, R., Lasala, S. & Jaubert, J.-N. On the imperative need to use a consistent α-function for the prediction of pure-compound supercritical properties with a cubic equation of state. en. *Fluid Phase Equilibria* 445, 45–53. doi:10.1016/j. fluid.2017.04.015 (august 2017).

39. Zielke, F. & Lempe, D. Generalized calculation of phase equilibria by using cubic equations of state. en. *Fluid Phase Equilibria* 141, 63–85. doi:10.1016/S0378-3812(97) 00197-0 (december 1997).

40. Privat, R., Jaubert, J.-N. & Le Guennec, Y. Incorporation of a volume translation in an equation of state for fluid mixtures: which combining rule ? which effect on properties of mixing ? en. *Fluid Phase Equilibria* 427, 414–420. doi:10.1016/j.fluid.2016.07.035 (november 2016).

41. Wong, D. S. H. & Sandler, S. I. A theoretically correct mixing rule for cubic equations of state. en. *AIChE Journal* 38, 671–680. doi:10.1002/aic.690380505 (may 1992).

42. Chabab, S., Coquelet, C. & Rivollet, F. Generalization of the Wong-Sandler mixing rule to a generic cubic equation of state: Examples of use for systems of industrial interest (Hydrogen, CCUS, refrigeration). *The Journal of Supercritical Fluids* 212, 106336. doi:https://doi.org/10.1016/j.supflu.2024.106336 (2024).

43. Renon, H. & Prausnitz, J. M. Local compositions in thermodynamic excess functions for liquid mixtures. en. *AIChE Journal* 14, 135–144. doi:10.1002/aic.690140124 (january 1968).

44. Fandiño, O., Trusler, J. M. & Vega-Maza, D. Phase behavior of (CO2+H2) and (CO2+N2) at temperatures between 218.15 and 303.15 K at pressures up to 15 MPa. en. *International Journal of Greenhouse Gas Control* 36, 78–92. doi:10.1016/j.ijggc.2015.02.018 (may 2015).

45. Streett, W. B., Heintz, A., Clancy, P. & Chokappa, D. Phase Equilibria in Hydrogen Binary Mixtures From 63 to 280 K and Pressures to 6000 Bars. en. *MRS Proceedings*
22, 105. doi:10.1557/PROC-22-105 (1983).

46. Tsang, C. Y. & Streett, W. B. Phase equilibria in the H2-CO system at temperatures from 70 to 125 K and pressures to 53 MPa. en. *Fluid Phase Equilibria* 6, 261–273. doi:10.1016/0378-3812(81)85008-X (1981).

47. Streett, W. & Calado, J. Liquid-vapour equilibrium for hydrogen + nitrogen at temperatures from 63 to 110 K and pressures to 57 MPa. en. *The Journal of Chemical Thermodynamics* 10, 1089–1100. doi:10.1016/0021-9614(78)90083-6 (november 1978).

48. Hong, J. H. & Kobayashi, R. Vapor-liquid equilibrium study of the hydrogen-methane system at low temperatures and elevated pressures. en. *Journal of Chemical & Engineering Data* 26, 127–131. doi:10.1021/je00024a007 (april 1981).

49. Chabab, S., Théveneau, P., Coquelet, C., Corvisier, J. & Paricaud, P. Measurements and predictive models of high-pressure H2 solubility in brine (H2O+NaCl) for underground hydrogen storage application. *International Journal of Hydrogen Energy* 45, 32206–32220. doi:https://doi.org/10.1016/j.ijhydene.2020.08.192 (2020).

50. Chabab, S., Kerkache, H., Bouchkira, I., Poulain, M., Baudouin, O., Moine, É., Ducousso, M., Hoang, H., Galliéro, G. & Cézac, P. Solubility of H2 in water and NaCl brine under subsurface storage conditions: Measurements and thermodynamic modeling. *International*
Journal of Hydrogen Energy 50, 648–658. doi:https://doi.org/10.1016/j. ijhydene.2023.10.290 (2024).

51. Jaeschke, M., Hinze, H. M., Achtermann, H. J. & Magnus, G. PVT data from burnett and refractive index measurements for the nitrogen—hydrogen system from 270 to 353
K and pressures to 30 MPa. en. *Fluid Phase Equilibria* 62, 115–139. doi:10.1016/03783812(91)87010-7 (january 1991).

52. Owuna, F. J., Chapoy, A., Ahmadi, P. & Burgass, R. Experimental (ρ,P,T) data of H2 + CH4 mixtures at temperatures from 277 to 398 K and pressures to 56 MPa.
International Journal of Hydrogen Energy 68, 979–997. doi:https://doi.org/10.
1016/j.ijhydene.2024.04.244 (2024).

53. Ben Souissi, M. A., Kleinrahm, R., Yang, X. & Richter, M. Vapor-Phase (p , ρ, T , x) Behavior and Virial Coefficients for the Binary Mixture (0.05 Hydrogen + 0.95 Carbon Dioxide) over the Temperature Range from (273.15 to 323.15) K with Pressures up to 6
MPa. en. *Journal of Chemical & Engineering Data* 62, 2973–2981. doi:10.1021/acs. jced.7b00213 (september 2017).

54. Mallu, B. V. & Viswanath, D. S. Compression factors and second virial coefficients of H2, CH4, xCO2+$(1 - x)$ H2, and xCO2+$(1 - x)$ CH4. en. *The Journal of Chemical Thermodynamics* 22, 997–1006. doi:10.1016/0021-9614(90)90189-W (1990).

55. Lozano-Martín, D., Moreau, A. & Chamorro, C. R. Thermophysical properties of hydrogen mixtures relevant for the development of the hydrogen economy: Review of available experimental data and thermodynamic models. *Renewable Energy* 198, 1398–1429. doi:10.1016/j.renene.2022.08.096 (1 october 2022).

56. Lozano-Martín, D., Martín, M. C., Chamorro, C. R., Tuma, D. & Segovia, J. J. Speed of sound for three binary (CH4+H2) mixtures from P=(0.5 up to 20) MPa at T=(273.16 to 375) K. *International Journal of Hydrogen Energy* 45, 4765–4783. doi:10.1016/j. ijhydene.2019.12.012 (7 february 2020).

57. van Itterbeek A. & van Doninck W. Measurements on the Velocity of Sound in Mixtures of Hydrogen, Helium, Oxygen, Nitrogen and Carbon Monoxide at Low Temperatures.
Proceedings of the Physical Society. Section B 62′ 62. doi:10.1088/0370-1301/62/1/ 308 (1 january 1949).

58. Karakatsani, E. & Aasberg-Petersen, K. Sustainable pathways to generate hydrogen:
A thermodynamic view. *Fluid Phase Equilibria* 578, 114011. doi:10.1016/j.fluid. 2023.114011 (1 march 2024).

59. Varzandeh, F., Stenby, E. H. & Yan, W. Comparison of GERG-2008 and simpler EoS models in calculation of phase equilibrium and physical properties of natural gas related systems. *Fluid Phase Equilibria* 434, 21–43. doi:https://doi.org/10.1016/j.fluid. 2016.11.016 (2017).

60. Alanazi, A., Ali, M., Bawazeer, S., Yekeen, N. & Hoteit, H. Evaluation of cubic, PCSAFT, and GERG2008 equations of state for accurate calculations of thermophysical properties of hydrogen-blend mixtures. *Energy Reports* 8, 13876–13899. doi:10.1016/ j.egyr.2022.10.257 (1 november 2022).

61. Beckmüller, R., Thol, M., Bell, I. H., Lemmon, E. W. & Span, R. New Equations of State for Binary Hydrogen Mixtures Containing Methane, Nitrogen, Carbon Monoxide, and Carbon Dioxide. *Journal of Physical and Chemical Reference Data* 50, 013102. doi:10.1063/5.0040533 (23 march 2021).